Quantum dot spectroscopy using a single phosphorus donor

Holger Büch, Martin Fuechsle, William Baker, Matthew G. House, and Michelle Y. Simmons

Quantum dot spectroscopy using a single phosphorus donor

Holger Büch, Martin Fuechsle, William Baker, Matthew G. House and Michelle Y. Simmons

Australian Research Council Centre of Excellence for Quantum Computation and Communication Technology, University of New South Wales, Sydney, New South Wales 2052, Australia.

Using a deterministic single P donor placed with atomic precision accuracy next to a nanoscale silicon quantum dot, we present a novel way to analyze the energy spectrum of small quantum dots in silicon by tunnel coupled transport measurements. The energy level structure of the quantum dot is observed as resonance features within the transport bias triangles when the donor chemical potential is aligned with states within the quantum dot as confirmed by a numeric rate equation solver, SIMON. This technique allows us to independently extract the quantum dot level structure irrespective of the density of states in the leads. Such a method is useful for the investigation of silicon quantum dots in the few-electron regime, where the level structure is governed by an intricate interplay between the spin- and valley-orbit degrees of freedom.

Recent advances in atomic-scale lithography have allowed the realization of a single atom transistor [1], achieved by deterministically placing a single P dopant with atomic precision between planar phosphorus doped leads. This controlled positioning of individual P dopants comprises a significant advance in the fabrication of quantum computer architectures in silicon [2,3], in which P donors naturally form spin qubits. The electronic spin state of the single electron qubit can be read out via spin-dependent tunneling between dopant atoms [4] and an in-plane quantum dot integrated as the island in a single electron transistor (SET) [5]. The fidelity of initialization and readout mechanisms, especially in a clocked fashion in a multi-qubit structure, critically relies on controlling the tunnel rate between the electron spin qubit and the SET dot which is sensitive both to the inter-dot distances and to the electronic structure of both the SET quantum dot and the donor. A thorough understanding of the quantum-mechanical level structure of these small SET quantum dots is therefore at the heart of the successful operation of single-electron devices for quantum computation and other applications, such as memory devices [6] or electron pumps for metrological purposes [7].

The electronic structure of an isolated quantum dot in the few-electron regime [8-11] is experimentally accessible using tunnel spectroscopy [12] and transport spectroscopy measurements [13]. Here the electronic structure can be determined from conductance variations as a function of source-drain and gate voltages. While this has proven a reliable tool for studying large SET devices, at the atomic scale it can be difficult to disentangle the electronic
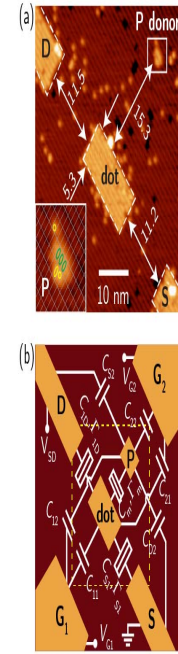

FIG. 1. **Single donor spectroscopy architecture.** (a) A filled state STM image of the lithographic template for a single donor, tunnel coupled to a quantum dot, in an SET architecture (with gates G_1 and G_2 outside of image size). Inset: Close-up of the single donor site, showing three clean dimers (green) suitable for the incorporation of a single P donor, while isolated clean dimers and single dangling bonds not able to incorporate phosphorous atoms are marked by yellow ellipses/circles. (b) An equivalent circuit model of the device, showing the positions of the in-plane gates G_1 and G_2, used for the rate equation model.
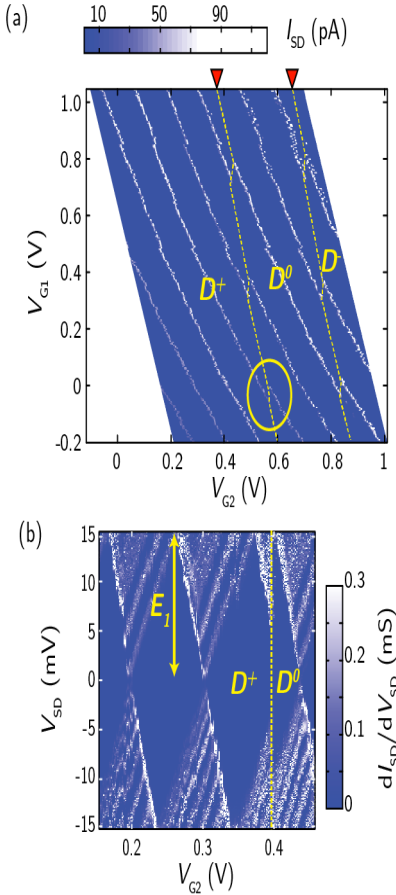
FIG. 2. **Charge stability diagram across the silicon quantum dot**. (a). A large-scale map of the SET current through the dot as a function of V_{G1} and V_{G2} for a fixed source-drain bias of V_{SD} = 1 mV. Two sets of discontinuities of the SET conduction lines are observed (red arrows) corresponding to the charge transitions D^+ ↔ D^0 and D^0 ↔ D^- on the single donor. (b) The SET conductance as a function of SD bias and G_2 voltage, showing Coulomb diamonds as well as excited state lines running parallel to the left edges of the diamonds. The donor charge transition D^+ ↔ D^0 results in a ∼ 20mV shift in gate voltage. E_1 is the charging energy of the quantum dot.

spectrum of the dot from those of the highly confined lead states, especially when the device system does not allow for tuning of the lead density of states independent of the quantum dot itself. This is in contrast to MOS devices where recent experiments have shown that they can disentangle the lead DOS by independently tuning their energy levels with a gate voltage [14].

We can circumvent this problem using a strongly tunnel coupled single P donor, precisely placed close to the SET quantum dot of interest to charge-sense the dot energy levels. Pierre *et al.* showed previously [15] that a tunnel coupled individual

charge trap such as a single dopant can give rise to differential conductance features in an SET stability diagram. These features are usually attributed to excited states in the SET dot or the leads, but the model adopted by Pierre *et al.* [15] neither captures the internal level structure of the SET dot nor of the leads. Johnson et al. demonstrated [16] excited-state spectroscopy of two large quantum dots by quickly aligning states of both quantum level structures via gate pulses, while the dots are not in electrical contact with the leads. In contrast to these two papers, we will show in this work, that a precisely placed single dopant can perform detailed spectroscopy of the level structure of the SET quantum dot alone, despite electrical contact with the leads and without the need for time resolved gate operations, thereby maintaining the ease of quantum dot transport measurements.

In Fig. 1a, we show a filled state STM-image of the lithographic template defining the inner part of the device, fabricated on a (2x1) reconstructed surface of a p-type Si substrate (1–10 Ωcm) in ultra-high vacuum. The Si surface is terminated with an atomic hydrogen layer which is then selectively patterned with an STM tip to form the device: leads (S and D), a quantum dot (∼5 x 10 nm^2, ∼120 donors) and a single donor (P). Electrostatic control gates (G_1, G_2) are fabricated along the axis between the dot and the donor, ∼50 nm away from the SET dot. After dosing with phosphine gas which only adsorbs to the exposed parts of the Si surface, phosphorus atoms are incorporated into the silicon crystal using a 60 s anneal to 330° C. The whole device is then encapsulated with ∼30 nm of epitaxial silicon at 250° C and a growth rate of ∼0.15 nm/min [17]. To ensure the deterministic incorporation of a single P atom, we desorb three adjacent Si dimers [1] (see inset of Fig. 1a) and note that spurious single dangling bonds in close proximity to the donor site cannot incorporate another P dopant [18]. By extracting the device capacitances from transport measurements, we can employ the equivalent circuit model of the device in Fig. 1b to simulate electron transport through the device. All device components are thus formed by laterally patterning with the STM and dosing with phosphine to form the single phosphorus atom (P) tunnel coupled to a densely packed phosphorus doped quantum dot with leads, and gates whose conductivity remain well above the metal-insulator-transition [19].

The presence of a single donor, tunnel-coupled to the quantum dot, can be observed in the charge stability map in Fig. 2a. Here we plot the current through the dot as a function of both gate voltages, V_{G1} and V_{G2}, at a constant SD bias of 1 mV, recorded at a base temperature of 50 mK. The parallel lines of high current shown in white at ~45° to the V_{G1}, V_{G2} axes occur when the electrochemical potential of the quantum dot, μ_1, is aligned with the Fermi level of the source and drain leads. The electron occupation number N_1 on the quantum dot increases by 1 as each conduction line is crossed towards higher gate voltages. These lines show discontinuities along two steep lines (yellow dotted lines), indicating the two charge transitions on the single donor, from the D^+ to the D^0 charge state and from the D^0 to the D^- state. The presence of only two discontinuities confirms that the only charge impurity that the SET quantum dot is sensitive to in the gate voltage space is the deterministically placed single P donor. Further evidence for this charge impurity to be a single donor was obtained by the measurement of its spin relaxation time (T_1) as a function of magnetic field. This measurement was performed by operating the charge impurity as a spin qubit in the way described in [4]. We found T_1 to increase proportionally to B^5, as predicted by Hasegawa *et al.* [20] for shallow donors in semiconductors. The proportionality factor was found to be $0.015 T^{-5}s^{-1}$, which is an exclusive value for an electron hosted by a single donor compared to larger donor clusters [21].

The single donor charge transition $D^+ \leftrightarrow D^0$ can also be observed as a charge offset in the Coulomb diamond plot in Fig. 2b (again marked by the vertical dashed yellow line). Here we also observe conductance features beyond the edges of blockaded SET current in the Coulomb diamonds, corresponding to excited states either of the leads or the SET quantum dot [8]. Since these conductance lines only appear parallel to the left edges of the diamonds, we can conclude that the quantum dot is much more strongly coupled to the source lead than to the drain lead [13]. This difference in dot coupling is attributed to the geometric disparity in the tunnel gap sizes (see Fig. 1a) where the gap aspect ratio (lead width / gap distance) ~2.11 for S-dot and ~2.17 for dot-D. Other contributions to this asymmetry could also arise from the difference in the distinct local densities of states near the Fermi edges of the two leads [22].

In Fig. 3a, we focus on the discontinuity in the SET current along the D^+ to D^0 charge transition of the single donor closest to zero $V_{G1,G2}$ gate voltage (yellow circle in Fig. 2a). We now apply a SD bias of 3 mV such that the triple points at the discontinuity of the high current line, where the electrochemical potentials of both the SET island, μ_1, and the donor, μ_2, are aligned with the Fermi levels of the leads, grow into bias triangles, as highlighted by the white dotted triangles in Fig. 3a. These bias triangles can be considered as analogous to transport through a parallel double dot, where for example Pauli spin blockade has recently been observed [23]. Within the lower bias triangle, we observe four linear conductance features in a high-resolution current map as seen in Fig. 3b (marked by yellow arrows), while the upper bias triangle is free of any such features. These line features are parallel to the mutual charge exchange line (indicated by the red dashed line in Fig. 3a), connecting the two triple points. As a consequence, we can attribute these vertical lines to resonances between the single donor ground state and different energy states within the quantum dot. In contrast, resonances between the levels of the SET quantum dot and the leads would occur in a high-resolution current map as current modulation features running parallel to the SET high current lines.

To explain the underlying mechanism leading to the occurrence of these line features, we examine the energy levels of the donor and the quantum dot involved in transport by reference to the schematic diagrams in Fig. 3c-e. In Fig. 3c, we consider 4 occupied energy levels in the quantum dot for the configuration $(N,0)$ where N corresponds to the number of electrons on the quantum dot and the 0 refers to zero electrons on the donor. Electron transport can occur through the dot as indicated by the red arrows. First an additional electron enters the dot from the source lead and subsequently an electron from any of the levels within the bias window can exit to the drain allowing the transport cycle to restart. The donor level however is not aligned with any of the dot levels ("Off resonance") and only has the role as a spectator.

If however, as depicted in Fig. 3d, the electrochemical potentials of one occupied level in the quantum dot within the bias window and that of the single donor are aligned ("On resonance") an electron from the dot can escape to the donor instead of to the drain of the SET (indicated by red arrow). This is particularly the case if there is

strong resonant coupling between the SET quantum dot and the donor (i.e., $\Gamma_m \sim \Gamma_{1D}$). Now all the quantum dot levels are lifted by the mutual charging energy E_m (see Fig. 3e) as the donor is now occupied by one electron. As a consequence, the quantum dot levels no longer reside within the bias window and electron transport through the quantum dot is not allowed. Depending on which quantum dot level is in resonance with the donor level, the quantum dot is left behind in an orbital-excited state after the electron transfer, from where it quickly relaxes to the ground state (indicated by red arrow). From here, the cycle can return to the starting point only when the electron at the single donor either escapes to the drain, which occurs at a much slower rate due to the larger distance between the donor and the drain or back to the dot. Since in the lower bias triangle the total observed SET current is proportional to the average fraction of the time the donor is unoccupied, the observed SET current is thus significantly reduced along the resonance lines. Reductions in the conductivity such as we see have also been explained using a model of a single charge trap [15]. However, for this to explain the features we see would require multiple accidental charge traps in the vicinity of the quantum dot, each with indistinguishable capacitive couplings to the gates, a possibility we find very unlikely.

We can derive the average energy separation of the states in the quantum dot, ΔE by knowing the effective gate lever arm, $\alpha \approx 0.15$ for tuning μ_2, which is obtained from a lever arm calibration experiment [24]. Here the gating efficiency of the two gates on the donor is measured while μ_1 is kept constant. We find $\Delta E = \alpha \Delta V \approx 0.5$ meV, where ΔV is the average separation of two consecutive resonances in gate voltage space. This average energy level separation is in good agreement with a simple estimation of the mean level spacing in the SET dot extracted from its electronic confinement, $\Delta E = \pi \hbar^2/(g m^* A) = 0.701$ meV. Here, 0.19 m_e is the effective mass in two dimensions (m_e is the electron rest mass), $A \approx 150$ nm^2 is the effective confinement area and $g = 12$ accounts for full spin and valley degeneracies.

We further confirm that the lines observed in the bias triangle correspond to electron energy levels in the quantum dot using SIMON, a multi-purpose simulator based on a rate equation model [25, 26]. To capture the essential properties of the single
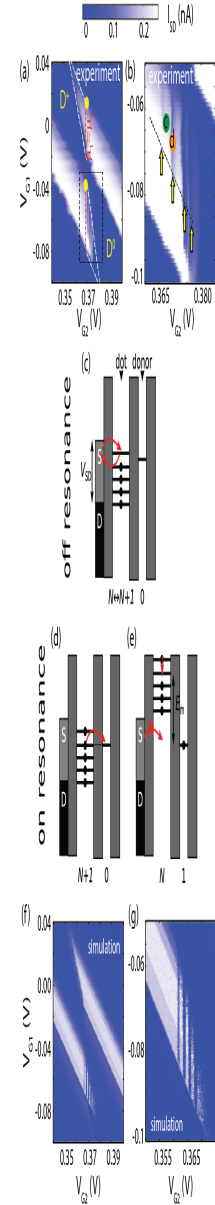

FIG. 3. **Visibility of quantum dot energy levels as resonance features in conductance bias triangles.** (a) A measured current map across the discontinuity indicated by the yellow circle in Fig. 2a, at a bias of V_{SD} = 3 mV. (b) A close-up of the lower bias triangle, at a bias of V_{SD} = 4 mV, revealing 4 line features of reduced current, marked by arrows. The two marked points correspond to the energy level diagrams in (c) and (d-e). (c) Energy level diagram representation of sequential SET transport in the lower bias triangle in the "Off resonance" position of the donor level. (d-e) Corresponding representation of suppressed SET transport in the lower bias triangle in the "On Resonance" position of the donor level. (f) An SET current map obtained from a SIMON simulation, revealing analogous vertical resonance features. (g) A close up of the resonance features in the lower bias triangle in (f).
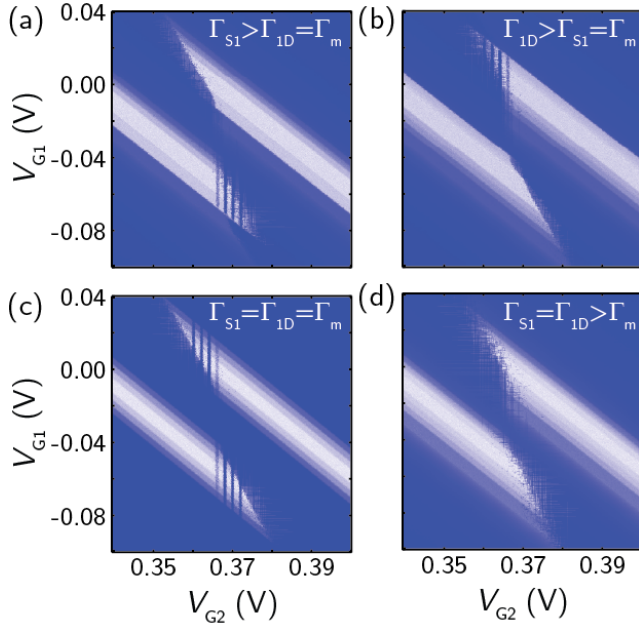
FIG. 4. **Effect of device asymmetry on the appearance of quantum dot energy levels**. (a)-(d) Simulated SET current maps around a donor charge transition for different ratios of the inter-dot tunnel rate, Γ_m, and the tunnel rates between the leads and the SET quantum dot, Γ_{S1} and Γ_{1D}. (a) For $\Gamma_{S1}>\Gamma_{1D}=\Gamma_m$ the occupied SET energy levels appear in the lower bias triangle. (b) For $\Gamma_{1D}>\Gamma_{S1}=\Gamma_m$ the empty SET energy levels become visible in the upper bias triangle (c) $\Gamma_{S1}=\Gamma_{1D}=\Gamma_m$, such that both occupied and empty SET energy levels become visible in the lower and upper bias triangle, respectively. (d) $\Gamma_{S1}=\Gamma_{1D}>\Gamma_m$, such that the SET energy levels are suppressed in both bias triangles.

donor spectroscopy device with SIMON, we simulate the equivalent circuit model in Fig. 1b. The appropriate device capacitances, $C_{11} = 0.74$ aF, $C_{12} = 0.14$ aF, $C_{21} = 1.18$ aF, $C_{22} = 0.59$ aF, $C_m = 0.36$ aF, $C_{\Sigma 1} = 5.92$ aF, and $C_{\Sigma 2} = 1.38$ aF can be extracted [27] from the current map in Fig. 2a and the charging energy of the quantum dot, which is given by the height of the diamonds in Fig. 2b ($E_1 = 15.2 \pm 0.2$ meV). From the height and the width of the Coulomb peaks at zero bias we can also estimate [28] the tunnel rate resistances between source and SET dot, Γ_{S1}, as ~1 GHz and between the SET dot and drain, Γ_{1D}, as ~10 MHz, respectively. Finally, for the tunnel resistance between quantum dot and the donor, Γ_m, we experimentally derive a lower boundary of ~2 MHz using the SET for time-resolved charge sensing of the single donor [17].

To simulate the current through the quantum dot we initially neglect the energy level structure in the leads and assume a constant density of states up to the Fermi edge. We specify a single energy level in the donor, the D^0 state, since the D^- state is located at ~44 meV, i.e. well above the D^0 state [29]. If we now consider a discrete set of energy states within the SET quantum dot with an equidistant level spacing of 0.5 meV as measured, we can simulate the current through the dot around a line discontinuity in the gate voltage space as shown in Figs. 3f and g. We observe linear conductance features in the lower bias triangle analogous to that observed in the experiment. Each of these lines can be attributed to one of the occupied energy levels of the quantum dot as per the mechanism illustrated in Fig. 3d. The simulation therefore confirms the origin of the linear conductance features in the bias triangles as the quantum dot energy levels.

Similarly, we would expect that empty states of the quantum dot would appear as linear conductance features in the upper bias triangle. The absence of these line features in the experiment (see Fig. 3a) and the simulation (see Fig. 3e) are intriguing. We will now demonstrate that the disparity of the upper and lower bias triangles can be explained by the asymmetry in the tunnel barriers between S-dot and dot-D in the device ($\Gamma_{S1} > \Gamma_{1D}$) which we already observed in the charge stability plot in Fig. 2b. In the upper bias triangle, electron transport through the SET quantum dot takes place when the donor is occupied by one electron. As discussed, this transport cycle is impeded if the interdot tunnel rate, Γ_m, is comparable to the usual loading rate of the SET dot, Γ_{S1}, while Γ_{1D} is irrelevant. Equivalently, in the lower bias triangle, current is allowed to flow through the quantum dot only while the donor remains unoccupied. Here, the transport cycle gets interrupted only when the electron leaves the SET quantum dot to the donor instead of through to the drain. Thus, to observe resonance lines within the lower bias triangle, Γ_m comparable to the usual emptying rate of the SET dot, Γ_{1D}, is required, while Γ_{S1} is irrelevant.

To illustrate how the relative tunnel rates influence the visibility of the resonance features, we produced rate equation models in SIMON, the results of which are shown in Fig. 4. In Fig. 4(a), we assume that the quantum dot is more strongly coupled to the source than to the drain $\Gamma_{S1} > \Gamma_{1D}$, as in the experiment. In agreement with the experiment, the resonance features appear only in the lower bias triangle. If the relative tunnel rates are reversed so that $\Gamma_{S1} < \Gamma_{1D}$, Fig. 4 (b), the resonance features shift to the upper bias triangle. In this case the

current is limited by electrons tunneling into the quantum dot, which can occur only while the donor is charged. In Fig. 4 (c) is a simulation with $\Gamma_{S1} = \Gamma_{1D}$, which shows that the resonance features can appear simultaneously in both triangles if the tunnel rates to the leads are equal. If resonant tunneling to and from the donor is slow, it does not influence the current significantly as shown in Fig. 4 (d), in which the features have disappeared as Γ_m is made to be small relative to the other rates, representing the usual regime such devices are operated in [4].

We have presented a single atom device where we have deterministically placed a single donor tunnel-coupled to a small quantum dot and used the donor as a spectrometer to probe the energy levels of the dot. From this study we have directly measured the average level separation within the quantum dot to be ~ 0.5 meV, and find this to be in good agreement with a simple particle in a box estimate. While the single donor placed as a tunnel-coupled sensor for the quantum dot thus constitutes the heart of the spectroscopic analysis presented here, we note that alternative ways for charge detection can be considered, such as capacitively coupling the quantum dot to be probed and the donor to an additional charge detector as in Ref. [16]. However, since our devices are ultimately being designed for single shot spin read out with high fidelity [4], the spectroscopic information we observe occurs conveniently as a by-product of the transport measurements. This result demonstrates how a single donor with a well-defined energy spectrum forms a powerful tool to extract quantum dot energy levels. Significantly it highlights that the observation of features in the transport bias triangles provide important information about the impact of asymmetry in the tunnel rates in the device. Such an analysis of tunneling rates in donor based devices will be useful in designing scalable qubit readout and initialization architectures.

[1] M. Fuechsle, J.A. Miwa, S. Mahapatra, H. Ryu, S. Lee, O.Warschkow, L. C. L. Hollenberg, G. Klimeck, and Michelle Y. Simmons, *A single-atom transistor,* Nat. Nanotechnol. 7, 242 (2012).

[2] B. E. Kane, *A silicon-based nuclear spin quantum computer*, Nature **393**,133 (1998).

[3] L. C. L. Hollenberg, A. D. Greentree, A. G. Fowler, and C. J. Wellard, *Two-dimensional architectures for donor-based quantum computing*, Phys. Rev. B **74**, 045311 (2006).

[4] H. Büch, S. Mahapatra, R. Rahman, A. Morello, and M. Y. Simmons, *Spin readout and addressability of phosphorus-donor clusters in silicon*, Nat. Commun. **4**, 2017 (2013).

[5] A. Fuhrer, M. Füchsle, T. C. G. Reusch, B. Weber, and M. Y. Simmons, *Atomic-scale, all epitaxial in-plane gated donor quantum dot in silicon*, Nano Lett. **9**, 707 (2009).

[6] L. J. Guo, E. Leobandung and S. Y. Chou, *A silicon single-electron transistor memory operating at room temperature*, Science **275**, 649-651 (1997).

[7] Y. Ono and Y. Takahashi, *Electron pump by a combined single-electron/field-effect- transistor structure*, Appl. Phys. Lett. **82** (8), 1221-1223 (2003).

[8] M. Fuechsle, S. Mahapatra, F.A. Zwanenburg, M. Friesen, M. A. Eriksson, M. Y. Simmons, *Spectroscopy of few-electron single-crystal silicon quantum dots*, Nat. Nanotech. **5**, 502 (2010).

[9] C. H. Yang, A. Rossi, R. Ruskov, N. S. Lai, F. A. Mohiyaddin, S. Lee, C. Tahan, G. Klimeck, A. Morello and A. S. Dzurak, *Spin-valley lifetimes in a silicon quantum dot with tunable valley splitting*, Nat. Commun. **4**, 2096 (2013).

[10] W. H. Lim, C. H. Yang, F. A. Zwanenburg and A. S. Dzurak, *Spin filling of valley-orbit states in a silicon quantum dot*, Nanotechnology **22** , 335704 (2011).

[11] Y. Hada and M. Eto, *Electronic states in silicon quantum dots: Multivalley artificial atoms*, Phys. Rev. B **68**, 155322 (2003).

[12] M. Thalakulam, C. B. Simmons, B. J. Van Bael, B. M. Rosemeyer, D. E. Savage, M. G. Lagally, Mark Friesen, S. N. Coppersmith, and M. A. Eriksson, *Single-shot measurement and tunnel-rate spectroscopy of a Si/SiGe few-electron quantum dot*, Phys. Rev. B **84**, 045307 (2011).

[13] L. P. Kouwenhoven, C. M. Marcus, P. L. McEuen, S. Tarucha, R. M. Westervelt, N. S. Wingreen: *Electron transport in quantum dots*, in L. L. Sohn, L. P. Kouwenhoven, G. Schon (eds.): NATO Advanced Study Institute on Mesoscopic Electron Transport, pages 105– 214 Curacao, Neth Antilles, Springer (1996).

[14] M. Mottonen, K. Y. Tan, K. W. Chan, F. A. Zwanenburg, W. H. Lim, C. C. Escott, J. M. Pirkkalainen, A. Morello, C. Yang, J. A. van Donkelaar, A. D. C. Alves, D. N. Jamieson, L. C. L. Hollenberg and A. S. Dzurak, *Probe and control of the reservoir density of states in single-electron devices*, Phys. Rev. B **81**, 161304 (2010).

[15] M. Pierre, M. Hofheinz, X. Jehl, M. Sanquer, G. Molas, M. Vinet and S. Deleonibus, *Background charges and quantum effects in quantum dots transport spectroscopy*, Eur. Phys. J. B **70**, 475-481 (2009).

[16] A. C. Johnson, C. M. Marcus, M. P. Hanson, A. C. Gossard, *Charge sensing of excited states in an isolated double quantum dot,* Phys. Rev. B **71**, 115333 (2005).

[17] S. Mahapatra, H. Buch, and M. Y. Simmons, *Charge sensing of precisely positioned P donors in Si*, Nano Lett. **11**, 4376 (2011).

[18] H. Wilson, O. Warschkow, N. Marks, N. Curson, S. Schofield, T. Reusch, M. Radny, P. Smith, D. McKenzie, and M.Y. Simmons, *Thermal dissociation and desorption of PH3 on Si(001): A reinterpretation of spectroscopic data*, Phys. Rev. B 74, 1 (2006).

[19] F. J. Ruess, L. Oberbeck, M. Y. Simmons, K. E. J. Goh, A. R. Hamilton, T. Hallam, S. R. Schofield, N. J. Curson, R. G. Clark. *Toward atomic-scale device fabrication in silicon using scanning probe microscopy,* Nano Lett. **4**, 1969 (2004).

[20] H. Hasegawa, *Spin-Lattice Relaxation of Shallow Donor States in Ge and Si through a Direct Phonon Process*, Phys. Rev. 118, 1523 (1960).

[21] Y. Hsueh, H. Büch, Y. Tan, Y. Wang, L. C. L. Hollenberg, G. Klimeck, M. Y. Simmons, and Rajib Rahman, *Spin-Lattice Relaxation Times of Single Donors and Donor Clusters in Silicon*, Phys. Rev. Lett. 113, 246406 (2014).

[22] H. Ryu, S. Lee, B. Weber, S. Mahapatra, L. C. L. Hollenberg, M. Y. Simmons, G. Klimeck, *Atomistic modeling of metallic nanowires in silicon*, Nanoscale **5**, 8666 (2013).

[23] B. Weber, Y. H. M. Tan, S. Mahapatra, T. F. Watson, H. Ryu, R. Rahman, L.C.L. Hollenberg, G. Klimeck, M. Y. Simmons, *Spin blockade and exchange in Coulomb-confined silicon double quantum dots*, Nat. Nanotech. **9**, 430 (2014).

[24] A. Morello, J. J. Pla, F. A. Zwanenburg, K. W. Chan, K. Y. Tan, H. Huebl, M. Möttönen, C. D. Nugroho, C. Yang, J. A. van Donkelaar, A. D. C. Alves, D. N. Jamieson, C. C. Escott, L.C.L Hollenberg, R. G. Clark, A. S. Dzurak, *Single-shot readout of an electron spin in silicon*, Nature **467**, 687 (2010).

[25] C. Wasshuber, H. Kosina, and S. Selberherr, *A compact analytical model for asymmetric single-electron tunneling transistors*, IEEE Trans. Comput. Aided Design **16**, 937 (1997).

[26] H. Inokawa, Y. Takahashi, *A compact analytical model for asymmetric single-electron tunneling transistors*, IEEE Trans. on Elec. Dev. **50**, 455 (2003).

[27] G. Yamahata, Y. Tsuchiya, S. Oda, Z. A. K. Durrani, H. Mizuta, *Control of electrostatic coupling observed for silicon double quantum dot structures*, Jap. J. of Appl. Phys. **47**, 4820 (2008).

[28] C. W. J. Beenakker, *Theory of coulomb-blockade oscillations in the conductance of a quantum dot*, Phys. Rev. B **44**, 1646−1656 (1991).

[29] A. Ramdas and S. Rodriguez, *Spectroscopy of the solid-state analogues of the hydrogen atom: donors and acceptors in semiconductors*, Rep. on Prog. in Phys. **44**, 1297 (1981).